Heliyon 11 (2025) e41315

Contents lists available at ScienceDirect

Heliyon

journal homepage: www.cell.com/heliyon

Research article

First-principles investigation of half-metallic $CaTGe_2O_6$ (T = Mn, Fe, Co) clinopyroxenes: Potential for spintronics and optoelectronics applications

Tasmi Akter [a], Jahirul Islam [a,*], Kamal Hossain [b], Rabeya Akter Rabu [c]

[a] Department of Materials Science and Engineering, Khulna University of Engineering & Technology, Khulna-9203, Bangladesh
[b] Department of Physics, Khulna University of Engineering & Technology, Khulna-9203, Bangladesh
[c] Department of Physics, Bangladesh Army University of Science and Technology, Khulna, Bangladesh

ARTICLE INFO

Keywords:
DFT
Clinopyroxene
Ferromagnetic
Half-metallic
Spintronics
Optoelectronics

ABSTRACT

Clinopyroxene is a subgroup of pyroxene that is found in a variety of igneous and metamorphic rocks. This study investigates the structural, mechanical, electronic, optical, and thermal characteristics of $CaTGe_2O_6$ (T = Mn, Fe, Co) using density functional theory. These structures' lattice parameters have been optimized using GGA-PBE, GGA-PBESOL, and LDA exchange-correlation functionals, where all these structures are found to be stable in monoclinic symmetry having a little variation with experimental results. All the structures are mechanically stable and ductile in nature. The $CaFeGe_2O_6$ has the highest melting point and Debye temperature among the three structures. The electronic band diagram and spin-polarized PDOS of these structures confirm the half-metallic nature of all three structures. The half-metallic band gaps of $CaTGe_2O_6$ (T = Mn, Fe, Co) are 3.05, 1.69, 1.99 eV in GGA + U and 2.88, 1.52, 1.78 eV in the LDA + U method, respectively. $CaMnGe_2O_6$ is metallic in the spin-up state, whereas both $CaFeGe_2O_6$ and $CaMnGe_2O_6$ are metallic in the spin-down state. Refractive indices and dielectric functions of these structures ensure the transparency of $CaTGe_2O_6$ (T = Mn, Fe, Co) clinopyroxenes around 28.5 eV photon energy. These structures possess the highest reflectivity and absorption coefficients in the UV region. These salient features of these structures suggest that the spintronics and optoelectronics industries may benefit from these clinopyroxene structures in the future.

1. Introduction

Pyroxenes are quasi-one-dimensional single-chain structures with the generic formula XYZ_2O_6, where X stands for single- or double-valent alkali or alkaline earth metals, Y denotes double- or triple-valent transition metals, and Z for Aluminum (Al), Germanium (Ge), or Silicon (Si) [1]. Approximately one-fifth of the lithosphere and 400 km or more of the upper mantle comprises pyroxenes. Additionally, they have been identified in objects from outer space, including meteorites and the surfaces of the moon and Mars [2]. For physical study, pyroxenes constitute a broad and flexible class of materials. Multiferroic materials with simultaneous ferromagnetism, ferroelectricity, and ferroelasticity are a potential family of pyroxenes. Unfilled d-orbitals are necessary for ferroelectricity, whereas partially occupied d-orbitals often lead to ferromagnetism [3,4]. The crystal structure has a unique arrangement that joins the

* Corresponding author.
E-mail address: jahirul@mse.kuet.ac.bd (J. Islam).

https://doi.org/10.1016/j.heliyon.2024.e41315
Received 28 August 2024; Received in revised form 12 December 2024; Accepted 17 December 2024
Available online 17 December 2024

corner-sharing ZO_4 tetrahedral chains with the chains of edge-sharing YO_6 octahedra. This arrangement is responsible for its multiferroicity [5]. Potential applications for these substances include data storage [6], spintronics [7], and sensor technologies [8].

Depending on its stacking condition, pyroxene can be a monoclinic or orthorhombic crystal system. Between these two crystal systems, the monoclinic one is called clinopyroxene. Two groups of clinopyroxene structures depend on the X-site atoms and Y-site atoms. The x-site is occupied by single-valent atoms such as Na^{1+} or Li^{1+}, and the Y-site adopts trivalent cations such as Fe^{3+}, Al^{3+}, Cr^{3+}, and Ni^{2+} in the 1:3 clinopyroxene group. Whereas the x-site adopts di-valent atoms such as Ca^{2+}, Sr^{2+}, and Y-site are occupied by di-valent transition metal cations such as Mg^{2+}, Co^{2+}, Fe^{2+}, and Ni^{2+}, in the 2:2 clinopyroxene group [9]. Clinopyroxenes show low-dimensional magnetic (quasi-one-dimensional) and spin gap behavior [10]. $LiTi^{3+}Si_2O_6$ and $NaTi^{3+}Si_2O_6$ [11,12], $LiV^{3+}Ge_2O_6$ [13], and $CaCuGe_2O_6$ [14] have undergone extensive research in terms of their low-dimensional magnetic behavior. Neutron diffraction research demonstrates the multiferroic behavior of Ge-based clinopyroxenes such as $NaFeGe_2O_6$ [4]. According to research by Jodlauk et al. [15], $LiCrSi_2O_6$, $NaFeSi_2O_6$, and $LiFeSi_2O_6$ all exhibit ferroelectricity in a magnetically ordered state. It is hard to get intriguing magnetic characteristics from pyroxenes based on magnesium because they exhibit relatively weak magnetic interaction. Sr^{2+} will provide fascinating multiferroic properties in the optoelectronic sector since it has a wider cationic radius than Ca^{2+} and Mg^{2+} [16].

Even though clinopyroxenes have lately attracted attention due to their fascinating low-dimensional magnetic and half-metallic behavior, just a handful of these materials have had the entire theoretical and computational investigation of structural, mechanical, electronic, and optical characteristics [17]. According to recent investigations of density functional theory (DFT), pyroxene nanosilicates have been shown to have moderate to high hydroxylation [18]. Several clinopyroxenes have been used in Li-ion batteries [19]. Other research has demonstrated that the substitution of Tl^{3+} for Al^{3+} in $NaAlSi_2O_6$ resulted in a significant bandgap decrease (from 5.32 eV to 2.05 eV), making this pyroxene a suitable component for solar and optoelectronic devices [20]. Ding et al. [21] have explored the synthesis and magnetic characteristics of $SrCoGe_2O_6$ and $SrMnGe_2O_6$. F. Fakhera et al. [16] investigated the effect of Y^{2+} (Y= Mn, Fe, and Co) on the physical properties of the $SrYGe_2O_6$ by the DFT method. This study reveals that all three compounds are half-metallic and ferromagnetic, show high photon absorption, and high reflectivity at a specific energy (13 eV) making them potential for optoelectronics and spintronics. A first principle investigation was carried out by Shahed et al. [22] to understand the effect of X^{1+} (X = Li, Na, K) on the structural, optical-electronic, and mechanical characteristics of $XFeSi_2O_6$ clinopyroxene. All three substances are found to be ferromagnetic half-metals with a magnetic moment of 5.0 μ_B. Their high melting temperature and Debye temperature make them suitable for good heat conductors.

Hydrothermal synthesis of some Ca-based 2:2 clinopyroxenes $CaFeSi_2O_6$ and $CaMGe_2O_6$, (M = Ni, Co, Mn), and magnetic characterization was performed by G.J. Redhammer et al. [23] to investigate their low-temperature magnetic characteristics and spin structure. The magnetic structures of the Fe, Co, and Ni clinopyroxenes are very similar, featuring collinear ferromagnetic spin coupling (FM) within the infinite edge-sharing octahedral chains and antiferromagnetic coupling (AFM) between them. $CaCoGe_2O_6$ and $CaNiGe_2O_6$ exhibit magnetic ordering at temperatures below 18K. G.J. Redhammer et al. [24] synthesized $CaFeGe_2O_6$ in evacuated Silica glass tubes to explore its crystal structure and magnetoelectronic behavior. They collected powder diffraction data within the temperature range (4K–300K) to analyze magnetic spin configuration, crystal structure, and temperature-dependence evolution. Interactions like FM within the octahedral chains and AFM between the chains are shown by the description of the magnetic spin structure. The magnetic moment's temperature dependency revealed that it saturated below 10K. E Lambruschi et al. [25] reported the studies of Raman spectra of $CaMGe_2O_6$ (M = Mg, Mn, Co, Fe, Zn, Ni) to explain the relations between crystal structures and vibrational modes. The main peaks correspond to tetrahedral stretching and chain bending modes, where the primary stretching mode displays wavenumber shifts due to M^{2+} substitution, though these shifts do not correlate with the M^{2+} cation's mass or size. Conversely, the chain bending wavenumber decreases linearly as the ionic radius of the M^{2+} increases. However, these experimental studies have primarily focused on individual properties such as magnetic behavior or structural properties, there is no comprehensive investigation into the mechanical, electronic, optical, and thermal properties of these compounds. First-principles DFT was used to study the structural, mechanical, elastic, thermal, and optoelectronic characteristics of Ca and Si-based clinopyroxenes $CaMSi_2O_6$ (M = Co, Fe, Mn) in the monoclinic phase. Studying the optoelectronic characteristics of Ca and Si-based clinopyroxenes reveals their ferromagnetic and half-metallic behavior. These materials also exhibit excellent machinability, increased Vickers hardness, high melting points, and Debye temperatures. Their study concludes that these compounds show strong potential for future applications in optoelectronic and plasmonic fields [17].

From the literature review discussed above, our interest in these compounds stems from their promising potential in spintronic and optoelectronic applications. The unique half-metallic nature of these materials, combined with their structural stability, suggests that they could be ideal candidates for spintronic devices where robust magnetic and electronic properties are essential. Additionally, clinopyroxenes exhibit intriguing electronic and magnetic behavior due to the interaction of transition metal ions (Mn, Fe, Co) with the crystal lattice, which can lead to novel spin-polarized conduction mechanisms. As far as we know there was no computational and theoretical analysis of the structural, mechanical, thermal, optical, and electronic properties of $CaTGe_2O_6$ (T = Mn, Fe, Co) clinopyroxenes. Our study offers a comprehensive exploration of these materials' structural, mechanical, electronic, optical, and thermal properties using first-principles calculations that have not been fully examined in prior work. By presenting detailed insights into these properties, our results provide a foundation for assessing the practical applicability of $CaTGe_2O_6$ (T = Mn, Fe, Co) compounds in real-world spintronic and optoelectronic technologies.

2. Methodology

We have used the Cambridge Serial Total Energy Package (CASTEP) program [26] with different functionals to perform the

structural, mechanical, thermal, optical, and electronic characteristics of the monoclinic $CaTGe_2O_6$ (T = Mn, Fe, Co) clinopyroxenes with space group *C*2/*c* in the monoclinic symmetry. The BFGS (Broyden Fletcher-Goldfarb-Shanno) [27] method has been used for optimizing structures and finding ground-state energy. BFGS method is a quasi-Newton optimization technique that approximates the inverse of the Hessian matrix to iteratively update the atomic positions, minimizing the total energy of the system. By minimizing the forces on atoms and achieving a local energy minimum, BFGS plays a crucial role in providing optimized structures that are essential for understanding material properties and guiding experimental efforts. These pseudo-atomic computations were performed using valence electron configurations: $2s^2\ 2p^4$ for O, $4s^2$ for Ca, $4s^2\ 4p^2$ for Ge, and 3 $d^5\ 4s^2$ for Mn, 3 $d^6\ 4s^2$ for Fe, and 3 $d^7\ 4s^2$ for Co atoms. The energy change per atom was 1×10^{-5} eV, the residual force was set to a maximum of 0.03 eV/Å, the maximum displacement of atoms was set to 0.001 Å, and maximum stress convergence thresholds were set at 0.05 GPa for the lattice constants and atomic position to be optimized appropriately. After several trials of cut-off energies, the cut-off energy was chosen at 500 eV with ultrasoft pseudopotential that denotes closely packed electron-ion interaction. The exchange-correlation energies were computed using the local density approximation (LDA), PBE (Perdew-Burke-Erzenhof), and PBE for Solids (PBESOL) method of the generalized gradient approximation (GGA) [28]. The structural properties were calculated using LDA, GGA-PBE, and GGA-PBESOL functionals and compared with experimental results. In the Brillouin zone of the unit cell, we optimized structures using the $4 \times 8 \times 8$ Monkhorst-Pack grid [29]. We have used GGA-PBESOL functionals to estimate mechanical properties, as GGA-PBESOL functionals offer more accuracy when examining the elastic and mechanical characteristics of materials compared to other functionals [30]. 13 elastic constants C_{ij} were obtained here using stress-strain relation for monoclinic crystal taking symmetry considerations. These elastic constants were used in further calculations of other mechanical properties. In the presence of transition metals, the GGA-PBE scheme underestimates the electronic characteristics. So, DFT + U approximations were used for the optimized crystal structures to get insight into the electronic properties (GGA + U, and LDA + U) and optical characteristics (GGA + U) of the $CaTGe_2O_6$ (T = Mn, Fe, Co) clinopyroxenes. Optical properties were examined using k-points of $10 \times 12 \times 12$ Monkhorst-Pack grid for better results. The Hubbard U parameter is critical in accounting for the electron-electron interaction in transition metals within density functional theory (DFT) calculations. For Mn, Fe, and Co, recent studies have explored their U values in various material contexts. For Mn, in doped BiTeI, the U value significantly influences magnetic properties, showing a magnetic moment decrease from 3 μ_B to 1 μ_B as U increases from 0 to 3 eV, indicating its role in ferromagnetic semiconductors [31]. Similarly, studies on Fe and Mn in half-metallic and ferromagnetic compounds reveal variations in magnetic moments and electronic structure with U ranging between 1 and 5 eV. These variations impact the coupling between atoms, altering properties such as metallicity and semiconducting behavior [32]. For Co, particularly in compounds like Co_2MnGe, the U parameter shows minimal influence on magnetic moments, suggesting robust electronic behavior in comparison to Mn and Fe [32]. Overall, these studies emphasize that the Hubbard U values are material-specific and depend significantly on the surrounding electronic and atomic structure. In our study, the Hubbard U value was set to 2.5 eV for Mn-3d, Fe-3d, and Co-3d orbitals to match the magnetic moment with experimental work.

3. Results and discussion

3.1. Structural properties

Pyroxenes are a type of polycrystalline material that is prevalent and possesses the generic formula XTZ_2O_6 [17]. In this study, we have focused on $CaTGe_2O_6$ (T = Mn, Fe, Co), which are clinopyroxene structures in a monoclinic phase having space group *C*2/*c*. These Ca-based clinopyroxenes contain three different lattice parameters (*a*, *b*, and *c*) and three lattice angles (α, β, and γ), among them α and γ are at right angles) and β is different. In this clinopyroxene structure, the X-site atom is Ca^{2+}, the T-site atom is Mn^{2+}, Fe^{2+} or Co^{2+}, Z-site atom is Ge^{4+}. The optimized crystal structures of $CaTGe_2O_6$ clinopyroxene are shown in Fig. 1, which is made up of [-TO_6-] edge-sharing octahedra. Tetrahedral [-GeO4-] chains of Germanium and Oxygen are joined by octahedral stacking of T-site cations [24,33]. The channels made by stacking octahedra and tetrahedra chains contain the Ca^{2+} cations. The tetrahedral-octahedral-tetrahedral (TOT) stacking of $CaTGe_2O_6$ is repeated in the same direction, which is the reason for all these clinopyroxenes being monoclinic structures. The experimental values of structural parameters of the $CaTGe_2O_6$ from the literature are

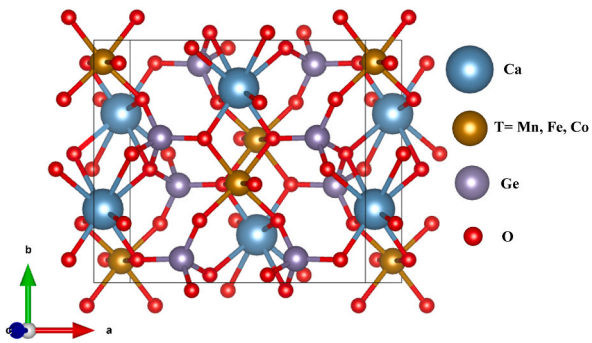

Fig. 1. Optimized crystal structure of the $CaTGe_2O_6$ (T = Mn, Fe, Co) clinopyroxenes.

tabulated in Table 1. The optimized unit cells lattice parameters and volume using different exchange-correlation functionals are also tabulated in Table 1 to compare with the experimental results. We have found the structural parameters and magnetic ordering of $CaMnGe_2O_6$ and $CaCoGe_2O_6$ from the study performed by G.J. Redhammer et al. [23]. They performed the hydrothermal synthesis of these compounds. From their study, the volume of $CaMnGe_2O_6$ and $CaCoGe_2O_6$ are 497.26 $Å^3$ and 476.77 $Å^3$ where calculations using GGA-PBESOL give the volumes of 500.52 $Å^3$ and 474.93 $Å^3$ respectively. Here other functionals give more deviated results. The lattice parameters of $CaFeGe_2O_6$ have been taken from the study of the synthesis of $CaFeGe_2O_6$ in an evacuated silica glass tube [24]. We didn't find the volume of $CaFeGe_2O_6$ in this study or any other literature. However, there is little difference between the experimental data and the optimized lattice parameters, which can be scientifically accepted. Since DFT calculations are performed in 0 K whereas experimental synthesis is performed at higher temperatures [28,34]. The $CaMnGe_2O_6$ structure, which was optimized by GGA-PBE exchange-correlation functional, occupies the most significant volume, 519.726 $Å^3$. Contrarily, the $CaCoGe_2O_6$ structure using the LDA functional occupies the smallest volume, 446.481 $Å^3$. The value of the optimized lattice constant 'a' ranges from 10.0570 Å to 10.3984 Å, whereas 'b' has a value close to 'a' range from 8.7036 Å to 9.3302 Å. The lattice parameter 'c' is located between 5.2398 Å and 5.5167 Å. The optimized lattice angle (β) was between 102.884° and 104.518° with minimal deviation from experimental results. Furthermore, it is observed that the calculated lattice parameters using GGA-PBESOL functional are very close to the experimental results, whereas GGA-PBE functional overestimates and LDA functional underestimates.

Table 2 displays the computed ground state energy in the ferromagnetic (FM), antiferromagnetic (AFM), and non-magnetic (NM) orderings. We have found the lowest ground state energies for $CaFeGe_2O_6$, and $CaCoGe_2O_6$ in FM ordering and for $CaMnGe_2O_6$ in AFM ordering. The lowest ground state energy indicates these compounds' stability in the specific magnetic configuration. From the experimental work performed by G.J. Redhammer et al. [23], we found that $CaCoGe_2O_6$ shows a strong FM ordering within the octahedral chain which overlooks the AFM interaction between the octahedral chains. It makes this structure a strong ferromagnetic nature with a positive curie temperature. $CaFeGe_2O_6$ also shows dominating ferromagnetic interaction with positive curie temperature (18.6K). But in $CaMnGe_2O_6$, AFM ordering of Mn^{2+} spins occurred both within and between the octahedral chains, resulting in complete AFM ordering with negative curie temperature. Their findings are also inconsistent with our ground state energy results. However, we have conducted further properties calculations for all three structures in the FM ordering so that we can compare the results in the same configuration.

We have calculated the formation energy and cohesive energy of these compounds to confirm the structural stability of these compounds in the monoclinic phase. The simulated conventional unit cell of $CaTGe_2O_6$ contains 4 primitive cells. Formation and cohesive energies per atom are calculated using the following formula [35,36]:

$$\Delta E_f = \frac{[E_{total} - 4E_{Ca} - 4E_T - 8E_{Ge} - 24E_O]}{40} \tag{1}$$

$$\Delta E_{coh} = \frac{[4E_{Ca}(iso) + 4E_T(iso) + 8E_{Ge}(iso) + 24E_O(iso) - E_{total}]}{40} \tag{2}$$

Where, E_{total}, E_{Ca}, E_T, E_{Ge}, E_O represent the total ground state energies of $CaTGe_2O_6$, Ca, T = (Mn, Fe, Co), Ge, O atoms, respectively. $E_{Ca}(iso)$, $E_T(iso)$, $E_{Ge}(iso)$, $E_O(iso)$ are the total energies of isolated single Ca, T = (Mn, Fe, Co), Ge, O atoms, respectively. 40 stands for total number of atoms in unit cell. The formation energies are −1.97 eV/atom, −1.83 eV/atom, and −1.77 eV/atom of $CaMnGe_2O_6$, $CaFeGe_2O_6$, and $CaCoGe_2O_6$, respectively and cohesive energies are 7.02 eV/atom, 6.91 eV/atom, and 6.74 eV/atom, respectively, tabulated in Table 2. The negative formation and positive cohesive energies ensure the structural stability of these compounds.

3.2. Mechanical properties

The mechanical and elastic properties of materials are vital for the fabrication and use of several devices. The way a crystal responds to pressure, strain, and other applied forces is influenced by its elastic characteristics. Interatomic bonding, vibrational modes of lattice, physical stability, stiffness, hardness, ductility, brittleness, anisotropic behavior, thermal properties like thermal expansion,

Table 1
Lattice parameters of $CaTGe_2O_6$ (T = Mn, Fe, Co) clinopyroxenes.

Structures	Calculation	a (Å)	b (Å)	c (Å)	β (°)	Volume ($Å^3$)
$CaMnGe_2O_6$	GGA-PBE	10.3984	9.3302	5.5167	103.824	519.73
	GGA-PBESOL	10.3303	9.1135	5.4710	103.651	500.52
	LDA	10.1298	8.9270	5.3502	103.669	470.11
	Experimental [23]	10.2667	9.1452	5.4599	104.071	497.26
$CaFeGe_2O_6$	GGA-PBE	10.3571	9.0727	5.4187	103.072	495.99
	GGA-PBESOL	10.2964	8.8597	5.3631	102.884	476.92
	LDA	10.0865	8.7036	5.2398	103.057	448.10
	Experimental [24]	10.1778	9.0545	5.4319	104.263	–
$CaCoGe_2O_6$	GGA-PBE	10.3405	9.0918	5.4336	104.518	494.52
	GGA-PBESOL	10.2720	8.8760	5.3796	104.466	474.93
	LDA	10.0570	8.7109	5.2620	104.407	446.48
	Experimental [23]	10.1477	8.9518	5.4274	104.754	476.77

Table 2
Ground state energies in the Ferromagnetic (E_{FM}), Antiferromagnetic (E_{AFM}), and Non-magnetic (E_{NM}) orderings, along with calculated Formation energy (ΔE_f), and Cohesive energy (ΔE_{coh}).

Structures	Calculation	E_{FM} (eV)	E_{AFM} (eV)	E_{NM} (eV)	ΔE_f (eV/atom)	ΔE_{coh} (eV/atom)
$CaMnGe_2O_6$	GGA-PBE	−17988.81	−17988.91	−17980.14	−1.97	7.02
$CaFeGe_2O_6$	GGA-PBE	−18830.49	−18830.03	−18827.32	−1.83	6.91
$CaCoGe_2O_6$	GGA-PBE	−19539.12	−19538.60	−19537.21	−1.77	6.74

melting and Debye temperatures, and other solid-state characteristics are all significantly influenced by elastic characteristics [37,38]. So, calculating the elastic constants is crucial for completely understanding a material. Elastic constants (C_{ij}) apply Hook's law to relate the strain and stress components. There are 36 distinct elastic constants as a result of the linear relationship. Due to the symmetry operations, the monoclinic phase of clinopyroxene structures is composed of 13 distinct constants [39]. Using the GGA-PBESOL exchange-correlation functional, the 13 elastic constants of monoclinic $CaTGe_2O_6$ (T = Mn, Fe, Co) clinopyroxenes are calculated in this current work. Numerous studies in the literature demonstrate that GGA-PBESOL functionals offer more accuracy when examining the elastic and mechanical characteristics of materials [43]. These calculated elastic constants C_{ij} (GPa) are depicted in Table 3. To confirm the mechanical stability of the monoclinic structure, it is crucial to meet the following conditions according to "Born stability criteria" [40,41]:

$$C_{11} > 0,\ C_{22} > 0,\ C_{33} > 0,\ C_{44} > 0,\ C_{55} > 0,\ C_{66} > 0 \tag{3}$$

$$[C_{11} + C_{22} + C_{33} + 2(C_{12} + C_{13} + C_{23})] > 0 \tag{4}$$

$$(C_{33}C_{55} - C_{35}^2) > 0,\ (C_{44}C_{66} - C_{46}^2) > 0,\ (C_{22} + C_{33} - 2C_{23}) > 0 \tag{5}$$

$$[C_{22}\,(C_{33}C_{55} - C_{35}^2) + 2C_{23}C_{25}C_{35} - C_{23}^2C_{55} - C_{25}^2C_{33}] > 0 \tag{6}$$

$$\{2[C_{15}C_{25}\,(C_{33}C_{12} - C_{13}C_{23}) + C_{15}C_{35}(C_{22}C_{13} - C_{12}C_{23}) + C_{25}C_{35}(C_{11}C_{23} - C_{12}C_{13})] - [C_{15}^2\,(C_{22}C_{33} - C_{23}^2) + C_{25}^2\,(C_{11}C_{33} - C_{13}^2) + C_{35}^2\,(C_{11}C_{22} - C_{12}^2)] + C_{55}(C_{11}C_{22}C_{33} - C_{11}C_{23}^2 - C_{22}C_{13}^2 - C_{33}C_{12}^2 + 2C_{12}C_{13}C_{23})\} > 0 \tag{7}$$

The calculated elastic constants given in Table 3 met all these criteria, which indicate the mechanical stability of $CaTGe_2O_6$ (T = Mn, Fe, Co) clinopyroxenes.

Elastic constant C_{44} suggests the elastic stability of compounds in harsh environments like high temperature and high pressure [42]. Among the three materials, $CaMnGe_2O_6$ has the lowest C_{44}, and $CaFeGe_2O_6$ and $CaCoGe_2O_6$ possess almost the same C_{44} values, which indicates that these two structures are stiffer in harsh conditions compared to $CaMnGe_2O_6$. Using Voigt, Reuss, and Hill's (VRH) approximations, elastic characteristics of $CaTGe_2O_6$ (T = Mn, Fe, Co), clinopyroxenes have been calculated. These computed elastic properties including Bulk (B), Shear (G), Young's modulus (Y), Pugh's ratio (B/G), Poisson's ratio (σ), Anisotropic factor (A_G), Machinability index (μ_m), Cauchy pressure (Cp), Vickers hardness (H_V), and Tian Hardness ($H_{v,Tian}$) are summarized in Table 4. Bulk modulus indicates the material's resistance to volume deformation against compression. While assessing the VRH approximation, the Voigt (V) method yields the highest values of B and G, while the Reuss (R) approximation yields the lowest. The following equations provide an average value according to Hill's (H) approximation:

$$B_H = \frac{B_V + B_R}{2} \tag{8}$$

$$G_H = \frac{G_V + G_R}{2} \tag{9}$$

Table 3
Elastic constants of the $CaTGe_2O_6$ (T = Mn, Fe, Co) clinopyroxenes.

Elastic Constant, C_{ij} (GPa)	Structures		
	$CaMnGe_2O_6$	$CaFeGe_2O_6$	$CaCoGe_2O_6$
C_{11}	149.474	175.941	174.865
C_{22}	44.414	126.056	105.760
C_{33}	131.160	161.834	159.188
C_{44}	21.555	37.103	37.099
C_{55}	33.965	44.638	25.336
C_{66}	20.605	58.963	30.945
C_{12}	38.403	57.764	54.287
C_{13}	37.933	49.194	57.790
C_{15}	4.930	3.391	6.156
C_{23}	20.676	49.692	61.595
C_{25}	−27.682	−4.195	−1.078
C_{35}	2.724	12.208	12.200
C_{46}	15.714	0.679	10.346

Table 4
Calculated different types of mechanical properties using the elastic constants of the $CaTGe_2O_6$ (T = Mn, Fe, Co) clinopyroxenes.

Parameter	Symbol	Structures		
		$CaMnGe_2O_6$	$CaFeGe_2O_6$	$CaCoGe_2O_6$
Bulk Modulus	B_V (GPa)	57.675	86.348	87.462
	B_R (GPa)	16.863	84.645	82.832
	B_H (GPa)	37.269	85.496	85.147
Shear Modulus	G_V (GPa)	30.427	48.620	36.419
	G_R (GPa)	8.707	46.109	31.609
	G_H (GPa)	19.567	47.364	34.014
Young's Modulus	Y_V (GPa)	77.630	122.809	95.940
	Y_R (GPa)	22.285	117.070	84.126
	Y_H (GPa)	49.958	119.944	90.051
Poisson's Ratio	σ	0.277	0.266	0.324
Cauchy Pressure	C_P (GPa)	3.968	4.556	32.454
Pugh's Ratio	B/G	1.905	1.805	2.503
Anisotropy Factor	A_G	0.555	0.027	0.071
Kleinman Parameter	ζ	0.407	0.474	0.457
Vicker's Hardness	H_v	15.716	27.647	31.718
Machinability Index	μ_m	1.729	2.304	2.295
Tian Hardness	$H_{v,Tian}$	3.631	7.217	3.94

$CaCoGe_2O_6$ possesses more B_V value but less B_R than $CaFeGe_2O_6$. This means that, according to the Voigt approach, $CaCoGe_2O_6$ is more resistant to compressive pressure, whereas the Reuss approach suggests that $CaFeGe_2O_6$ has more resistance to volume deformation against compression. However, all three approximations suggest that $CaMnGe_2O_6$ has the lowest volume stiffness. Shear modulus assesses the resistance to shape deformation against shear stress. Young's modulus measures an elastic body's resistance to length changes and has a relation with the bonding nature of materials. Bulk modulus and Young's modulus can be obtained by following equations [43]:

$$B = \frac{C_{11} + 2C_{12}}{3} \tag{10}$$

$$Y = \frac{9GB}{3B + G} \tag{11}$$

$CaFeGe_2O_6$ structure shows the highest Shear modulus and Young's modulus among three clinopyroxenes, representing the most rigid structure that allows the directional bonding of atoms [44]. For all three structures, the Bulk modulus is always more prominent than the Shear modulus, which ensures that the Bulk modulus is the more dominant parameter for the mechanical stability of these structures. Bulk-to-shear modulus (B/G), often known as Pugh's ratio, reveals if a material is brittle or ductile. If the value of Pugh's ratio is more than 1.75, then the substance will be ductile; otherwise, it will be brittle. All three $CaTGe_2O_6$ (T = Mn, Fe, Co) clinopyroxenes Pugh's ratio has crossed this limit, so all of them are ductile. Poison's ratio (σ) of these structures also intensifies the evidence of the ductile behavior of these materials. Poison's ratio quantifies the material's lateral contraction to elongation. If the value of the σ is greater than 0.26, then the material will be ductile, and below this threshold value, the material will be brittle [45]. From the tabulated data in Table 4, the σ for $CaTGe_2O_6$ (T = Mn, Fe, Co) are 0.277, 0.266, and 0.324, respectively, which also justified their

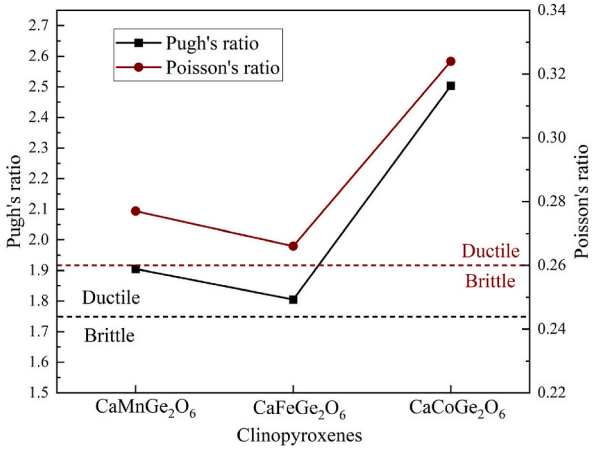

Fig. 2. Calculated Pugh's ratio and Poisson's ratio of $CaTGe_2O_6$ (T = Mn, Fe, Co) structures.

ductility. The ductile nature of these three compounds is shown in Fig. 2 from where it can be found that $CaCoGe_2O_6$ has the most considerable value of Pugh's ratio (2.503) and poison's ratio (0.324), which implies its highest ductility. Poison's ratio also provides predictions about how interatomic forces in materials will respond. Additionally, for non-central forces, σ will be in the range of 0.25–0.50 and fall outside of this range for central forces [51]. As the Poison's ratios of our investigated structures remain within this range, interatomic forces will be non-central for all three structures. Another parameter can also study materials' ductile and brittle behavior, Cauchy pressure (C_P), which is computed by the following formula [46,47]:

$$C_p = C_{13} - C_{55} \tag{12}$$

Positive Cauchy pressure indicates the ductile nature of the material, whereas a negative value denotes its brittle nature. All three clinopyroxenes have positive C_P values representing their ductile behavior, which is consistent with the results of the Poison's ratio and Pugh ratio. Additionally, it depicts the angular characteristics of atomic bonding in a material. If Cauchy's pressure is positive and significant, it suggests the existence of metallic bonding in any compound [47]. So, all $CaTGe_2O_6$ (T = Mn, Fe, Co) structures confirm the existence of metallic bonding.

The machinability index (μ_m) is used to assess the plasticity and lubrication properties of materials at the maximum economic state for machine operation. The machinability index can be expressed by the following formula [48]:

$$\mu_m = \frac{B}{C_{44}} \tag{13}$$

Machinability indices for $CaTGe_2O_6$ (T = Mn, Fe, Co) are 1.729, 2.304, and 2.295, respectively. $CaCoGe_2O_6$ shows better lubricating properties, lower friction, and the highest plasticity among the three structures, as it has the most extensive machinability index.

The Kleinman parameter (ζ), a dimensionless intrinsic strain parameter that describes resistance to stretching and bending of solids, is governed by the following equation below [49]:

$$\zeta = \frac{C_{11} + 8C_{12}}{7C_{11} + 2C_{12}} \tag{14}$$

The Kleinman parameter's value ranges from 0 to 1, where 0 indicates that external stress has less impact on bond bending. In contrast, $\zeta = 1$ denotes that structure bonds will face minimal stretching against applied external stress. The Kleinman parameters of the $CaTGe_2O_6$ (T = Mn, Fe, Co) are 0.407, 0.474, and 0.457, respectively, which ensures that these structures are more stable against bond bending than bond stretching when stress is applied.

Shear anisotropic factor (A_G) denotes the anisotropic nature of the crystal. Anisotropy refers to the material's capacity to show a distinct response in various directions to applied stresses, and isotropic nature indicates a uniform response in all directions. A_G can be computed using the formula below [50]:

$$A_G = \frac{G_v - G_R}{G_v + G_R} \tag{15}$$

When the anisotropic factor is strictly zero or nearer to zero, it confirms the material's isotropic behavior and further deviation from it specifies the anisotropic behavior [51]. Anisotropic factors of $CaTGe_2O_6$ (T = Mn, Fe, Co) clinopyroxenes listed in Table 4 indicate that $CaMnGe_2O_6$ has the highest anisotropic nature.

Vickers's hardness quantifies the material's hardness, meaning the material's resistance to elastic and plastic deformation against applied force [52]. There are various models in the literature that determine the theoretical Vickers's hardness of materials. However, among them, Tian Vickers's hardness model predicts the most reliable data on hardness for ductile materials. Tian Vickers's hardness model outperformed the other models and produced remarkably accurate findings when compared to the experimental results [53]. Thus, in this study, Vickers's hardness of $CaTGe_2O_6$ (T = Mn, Fe, Co) clinopyroxenes is determined using Tian's model.

$$H_{v,Tian} = 0.92\left(\frac{G}{B}\right)^{1.137} G^{0.708} \tag{16}$$

Tian Vickers's hardness of $CaTGe_2O_6$ (T = Mn, Fe, Co) clinopyroxenes tabulated in Table 4 indicates that $CaFeGe_2O_6$ has the highest hardness among the three clinopyroxenes.

3.3. Thermal properties

The melting point (T_m) measures the temperature at which the solid and liquid phases coexist in an equilibrium condition, and the temperature remains constant until the material has wholly melted. A material's binding energy is correlated with its melting temperature (T_m), which is inversely correlated with the thermal expansion coefficient. Melting temperature can be calculated using the following formula, which is related to the material's elastic constants [54]:

$$T_m = 345K + 4.5\left(\frac{K}{GPa}\right)\left(\frac{2C_{11} + C_{33}}{3}\right) \pm 300K \tag{17}$$

Among the three structures, $CaFeGe_2O_6$ and $CaCoGe_2O_6$ have comparatively high melting temperatures tabulated in Table 5, indicating that these two structures have strong covalent bonds. All these structures can be used in high-temperature applications due

to their high melting points.

Debye Temperature (θ_D) represents a crystal's largest normal mode of vibration. At Debye temperature, the thermal energy of the lattice vibrations is equivalent to the energy needed to break the bonds between atoms or molecules. It also indicates how much heat it can transmit and store in a material. The crystal lattice's atoms do not move much below the Debye temperature, enabling electrons to move across the lattice planes with a low electron-phonon interaction, leading to negligible scattering. Above the Debye temperature, the scattering rises dramatically, rendering a poor heat conductor material. Debye temperature is calculated using the following formula [55]:

$$\theta_D = \frac{h}{k_B} V_m \left(\frac{3n\rho N_A}{4\pi M} \right)^{\frac{1}{3}} \tag{18}$$

Here, h, V_m, n, ρ, k_B, M, and N_A represent Planck's constant, average sound velocity, total atoms in a molecule, density, Boltzmann's constant, molecular weight, and Avogadro's number, respectively. The calculated values of Debye Temperature of $CaTGe_2O_6$ (T = Mn, Fe, Co) clinopyroxenes are listed in Table 5, which are 275.955 K, 460.678 K, and 388.578 K, respectively. As $CaFeGe_2O_6$ possesses the highest Debye temperature, it can be a good heat conductor and thermally stable at higher temperatures compared to the other two structures; also, interatomic bonding will be more assertive in $CaFeGe_2O_6$.

In the fields of materials science, medicine, physics, geology, seismology, and musical instrument design, acoustic behavior like sound velocity is thought to be of great interest. Material's sound velocity also affects electronic and thermal conductivity. Transverse (V_T), longitudinal (V_L), and average sound wave velocity (V_m) can be expressed using the following equations [56]:

$$V_T = \sqrt{\frac{G}{p}} \tag{19}$$

$$V_L = \sqrt{\frac{3B + 4G}{3p}} \tag{20}$$

$$V_m = \left[\frac{1}{3} \left(2V_T^{-3} + V_L^{-3} \right) \right]^{-\frac{1}{3}} \tag{21}$$

Here, B, G, p denote the bulk modulus, shear modulus, and density of material respectively. From Tables 5 and it can be found that $CaFeGe_2O_6$ shows the highest transverse, longitudinal, and average sound velocity among the three structures.

3.4. Electronic and magnetic properties

Band structure and density of states (DOS) are crucial parameters in developing and manufacturing optoelectronic components. The band structure and DOS are examined of the optimized $CaMGe_2O_6$ (T = Mn, Fe, Co) clinopyroxene structures using DFT + U and LDA + U approximations to understand the electronic properties of these clinopyroxenes. The computed electronic band structures and DOS are depicted in Figs. 3 and 5, respectively. Due to the asymmetric nature of spin polarization, Fig. 3 shows two band structures for every $CaTGe_2O_6$ (T = Mn, Fe, Co) clinopyroxene at spin-up state and spin-down state. The Z-G-Y-A-B-D-E-C high symmetry points are shown in the band structures, and the dashed magenta straight line represents the Fermi level (E_F) at 0 eV photon energy. Fig. 3(a), (c), and 3(e) represent the electronic band structures at the spin-up state, and Fig. 3(b), (d), and 3(f) represent the band structures at the spin-down state of $CaTGe_2O_6$ (T = Mn, Fe, Co). The half-metallic band gaps of $CaTGe_2O_6$ (T = Mn, Fe, Co) are observed as 3.05 eV, 1.69 eV, and 1.99 eV using GGA + U, and 2.88 eV, 1.52 eV, and 1.78 eV using LDA + U, respectively. Moreover, all three clinopyroxenes show half-metallic properties. The band structure of $CaMnGe_2O_6$ in the spin-up state confirms its metallic nature as the valence band crosses the Fermi level in the spin-up state, and the valence or conduction bands do not touch the Fermi level in the spin-down state, indicating its semiconducting nature in the spin-down state. On the other hand, both $CaFeGe_2O_6$ and $CaCoGe_2O_6$ are metallic in the spin-down state and semiconducting in the spin-up state. The valence band maxima and conduction band minima are at the same point (G) for both the spin-up state and spin-down state for all these structures, indicating the direct band gap in the alpha spin channel band structure and the beta spin channel band structure. The half-metallic band gaps of $CaTGe_2O_6$ (T = Mn, Fe, Co) are listed in Table 6 and shown in Fig. 4 where all three compounds have comparatively higher band gaps in the GGA + U method than LDA + U. Here, $CaMnGe_2O_6$ has the highest half-metallic band gap among the three compounds.

Table 5
The resulting Debye temperature (θ_D), melting temperature (T_m), longitudinal sound wave velocity (V_L), transverse sound wave velocity (V_T), and average sound velocity (V_m) for $CaTGe_2O_6$ (T = Mn, Fe, Co) clinopyroxenes.

Structures	θ_D (K)	T_m ±300 (K)	V_L (m/s)	V_T (m/s)	V_m (m/s)
$CaMnGe_2O_6$	275.955	990.162	3840.086	2134.033	2376.731
$CaFeGe_2O_6$	460.678	1115.574	5738.251	3239.099	3581.368
$CaCoGe_2O_6$	388.578	1108.377	5344.184	2728.391	3056.883

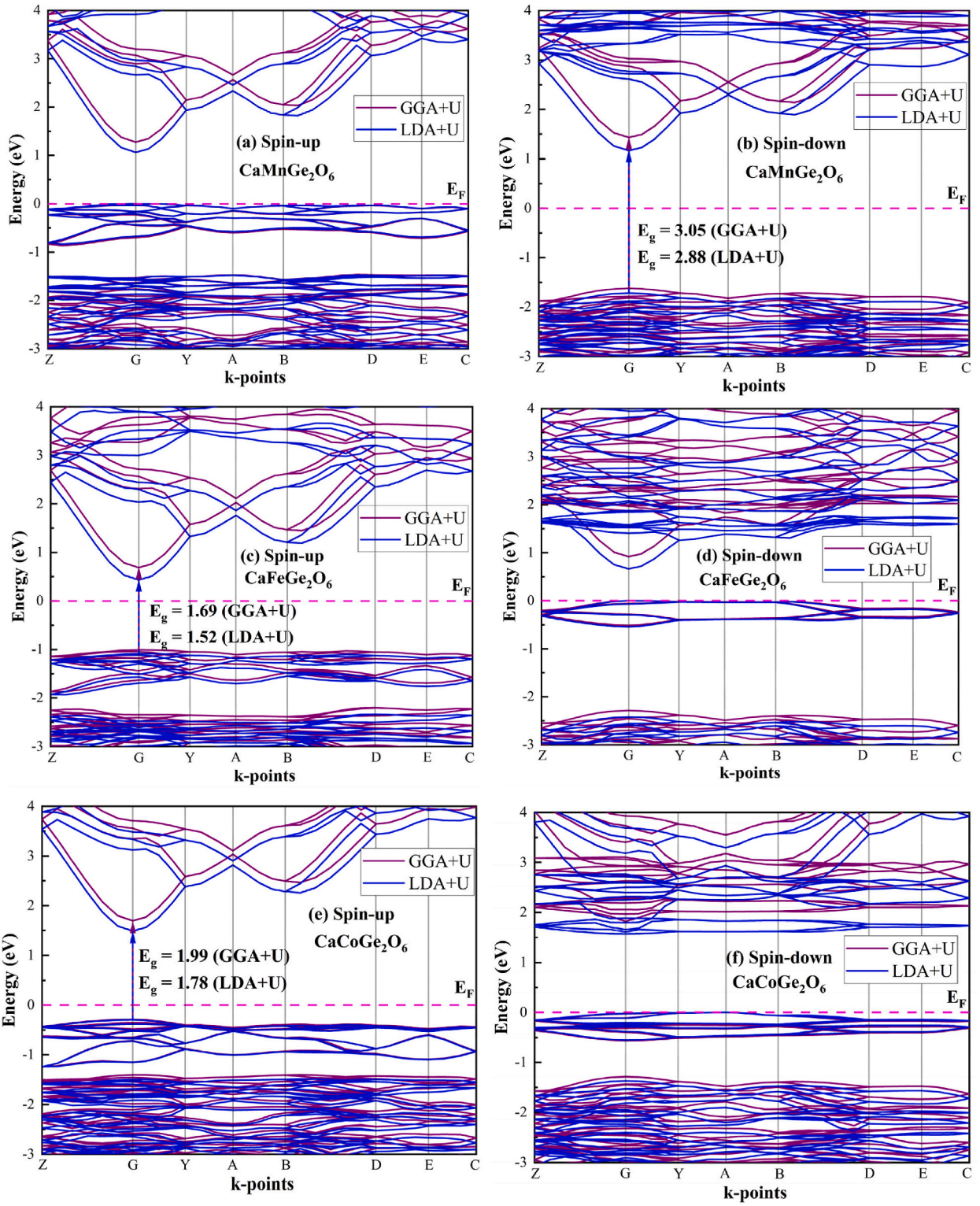

Fig. 3. Electronic band structures for (a) spin-up state and (b) spin-down state of $CaMnGe_2O_6$, (c) spin-up state and (d) spin-down state of $CaFeGe_2O_6$, (e) spin-up and (f) spin-down state of $CaCoGe_2O_6$, respectively using GGA + U and LDA + U methods.

Table 6
Half-metallic band gap and spin magnetic moment per unit cell (μ) of the $CaTGe_2O_6$ (T = Mn, Fe, Co) clinopyroxenes using GGA + U and LDA + U methods.

Structure	Half-metallic band gap		μ (μ_B)		
	GGA + U	LDA + U	GGA + U	LDA + U	Experimental
$CaMnGe_2O_6$	3.05 (↓)	2.88 (↓)	5.00	5.00	4.33 [23]
$CaFeGe_2O_6$	1.69 (↑)	1.52 (↑)	4.00	4.00	4.46 [23]
$CaCoGe_2O_6$	1.99 (↑)	1.78 (↑)	3.00	3.00	2.86 [24]

GGA + U and LDA + U methods give a similar pattern of the spin-polarized total density of states (TDOS) and partial density of states (PDOS) for each compound as shown in Fig. 5(a and b). From the PDOS of these clinopyroxenes, we observed that the Mn-3d, Fe-3d, Co-3d, and O-2p orbitals have a dominant existence adjacent to the Fermi level. O-2p orbital electrons dominate the valence band with a minor influence of Mn-3d, Fe-3d, and Co-3d orbitals electrons in three compounds. Ge-4p orbital electrons dominate the conduction band of three compounds with a minor contribution of Mn-3d, Fe-3d, and Co-3d orbital electrons. In the case of $CaMnGe_2O_6$, Mn-3d and O-2p orbitals travel through the fermi level, causing the valence band and conduction band to overlap in the alpha spin state, which also ensures its metallic nature in the alpha spin channel. When it comes to Fe-3d and Co-3d orbitals of $CaFeGe_2O_6$ and $CaCoGe_2O_6$, respectively, in the beta spin state, the valence band passes through the fermi level to the conduction band, revealing their metallic nature in the spin-down state. Following investigation of the PDOS, we concluded that the half-metallic behavior of the clinopyroxenes is caused by a substantial hybridization between the O-2p orbitals and the T (Mn, Fe, Co)-3d orbital.

The electronic characteristics of Mn, Fe, and Co transition metal atoms are influenced by the asymmetric distribution of electrons in their d-states. The existence of half-metallicity inside their electronic structures may be further explored using crystal field splitting theory (CFT). Coulomb interaction splits the d-orbital into dt_{2g} (d_{xy}, d_{yz}, d_{zx}) doublet orbitals at low energy and d_{eg} (d^2_{x-y}, d^2_z) doublet orbitals at high energy. Following Hund's law, the highest may $6e^-$ (3↑ spin and 3↓ spin) fit in the dt_{2g} orbitals, whereas the maximum $4e^-$ (2↑ spin and 2↓ spin) can fit in the d_{eg} orbital [16]. Mn, Fe, and Co have the electron configurations of [Ar] 3 d^5 $4s^2$, [Ar] 3 d^6 $4s^2$, and [Ar] 3 d^7 $4s^{2,}$ respectively. In Mn-atom, the first five electrons of the d_{2g} and deg orbital are of the same spin in the alpha spin state, and in Fe-atom, dt_{2g} has two unpaired electrons, and d_{eg} has two unpaired electrons in the alpha state. Co-atom comprises one unpaired electron in dt_{2g} orbital and two unpaired electrons in d_{eg} orbitals. So, the d_{eg} and d_{2g}, both doublet orbitals, remained unpaired in all three structures, which are responsible for magnetic interaction in these structures and metallic behavior in one spin state of all $CaTGe_2O_6$ (T = Mn, Fe, Co) clinopyroxenes.

To explore the magnetic interactions and half-metallic behavior, we have calculated the magnetic moment per unit cell in the Bohr magneton unit, tabulated in Table 6. The calculated total magnetic moment per unit cell for $CaMnGe_2O_6$, $CaFeGe_2O_6$, and $CaCoGe_2O_6$ are 5.00, 4.00, and 3.00 μ_B, respectively for both GGA + U and LDA + U calculation. The experimental magnetic moment from neutron diffraction results were 4.33, 4.46, and 2.86 μ_B for $CaMnGe_2O_6$, $CaFeGe_2O_6$, and $CaCoGe_2O_6$, respectively [23,24]. Our results are close enough to these experimental results. Integer values of the magnetic moment of these compounds indicate the potential for half-metallic behavior, as described by Slater Pauling's rule [57].

3.5. Optical properties

Materials' ground-state electronic structure has a significant impact on their optical characteristics. To explore optoelectronic

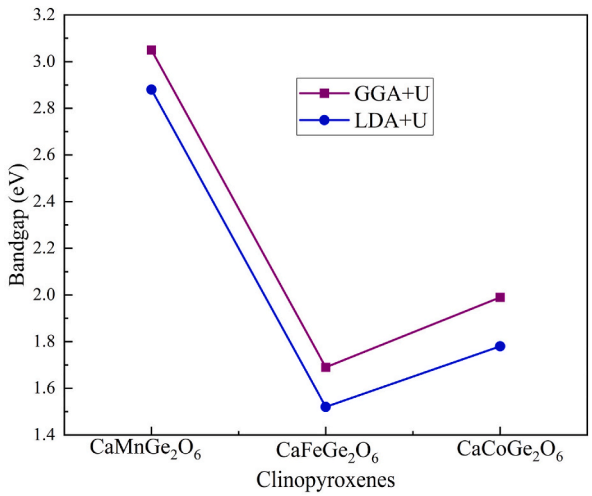

Fig. 4. Half-metallic band gap of $CaTGe_2O_6$ (T = Mn, Fe, Co) clinopyroxenes using GGA + U and LDA + U methods.

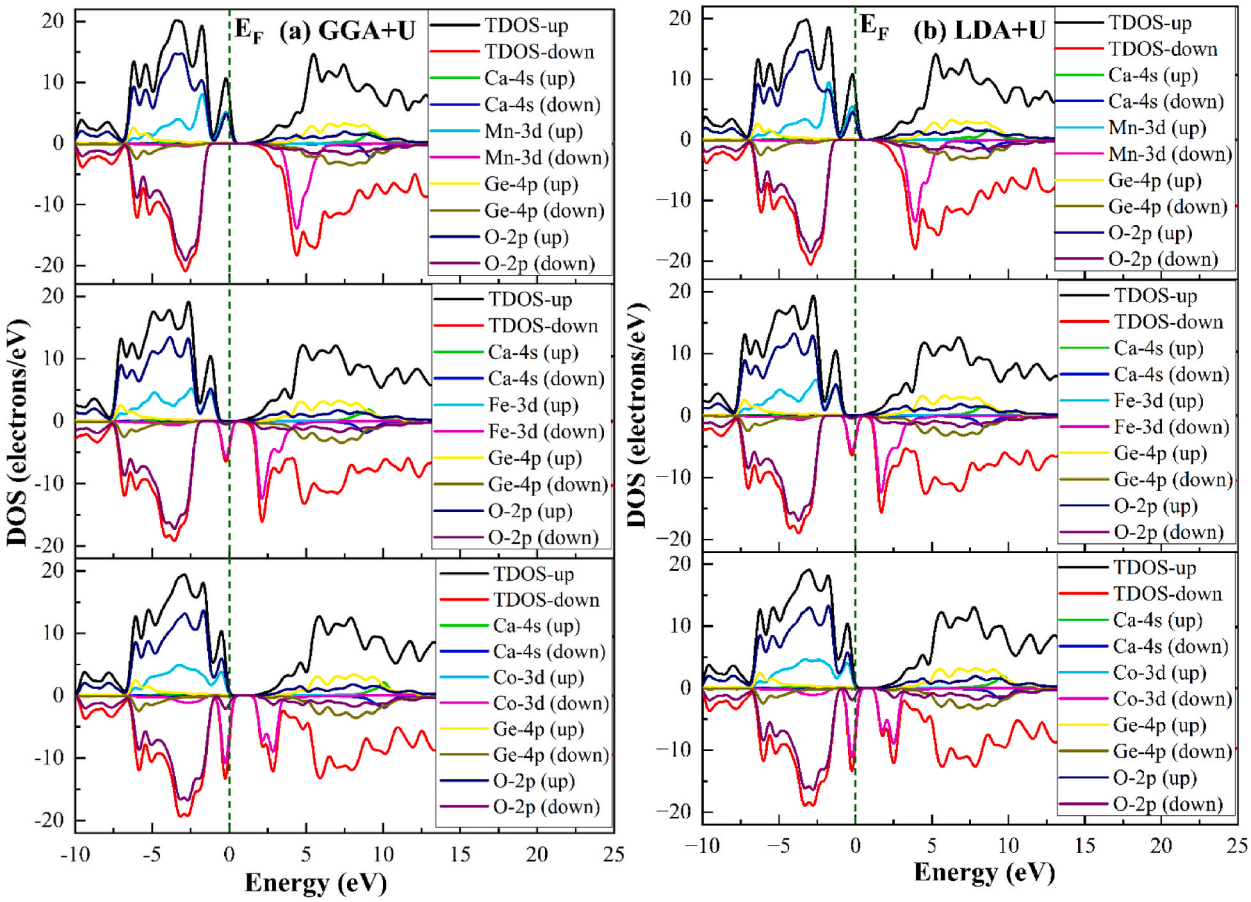

Fig. 5. Density of states utilizing (a) GGA + U and (b) LDA + U methods of the $CaMnGe_2O_6$, $CaFeGe_2O_6$, and $CaCoGe_2O_6$ clinopyroxenes from top to bottom, respectively.

applications, optical properties such as reflectivity, absorption coefficient, conductivity, dielectric function, refractive index, and loss function are detected up to 45 eV photon energy. In Fig. 6, the top layer indicates $CaTGe_2O_6$ (T = Mn, Fe, Co) clinopyroxenes photoconductive behavior and it is closely associated with its electronic conductivity. Conductivity measures the quantity of free charge carriers created due to bond breakage caused by the electron-photon interaction [58]. The photoconductivity graphs of these structures starting from 0 eV guarantee the absence of bandgap due to the hybridization of the valence and conduction bands in the up (alpha) spin state for $CaMnGe_2O_6$ or beta (down) spin state for $CaFeGe_2O_6$ and $CaCoGe_2O_6$. The maximum photoconductivity of these clinopyroxenes is almost similar. As the photon energy increases, conductivity also increases reaching around 4.25 1/fs at around 10 eV, after which it steadily declines as photon energy rises. However, again conductivity shows the highest peaks of 4.40 1/fs at about 26.30 eV and goes to zero at about 44 eV.

The bottom layer of Fig. 6(a and b) shows the frequency-dependent real and imaginary part of the refractive index of the $CaTGe_2O_6$ (T = Mn, Fe, Co) clinopyroxenes up to 45 eV photon energy. The frequency-dependent refractive index with a real part, $n(\omega)$, and an imaginary part, $k(\omega)$ can be mathematically stated as,

$$N(\omega) = n(\omega) + ik(\omega) \tag{22}$$

Here, $k(\omega)$ is the extinction coefficient, which displays the reduction of incident light while passing through the material, and $n(\omega)$, depicts the incident electromagnetic wave phase velocity inside the material. $CaFeGe_2O_6$ and $CaCoGe_2O_6$ possess the highest refractive index among the three structures, which is 2.33 at 4.08 eV, and the maximum refractive index for $CaMnGe_2O_6$ is 2.22 at 3.90 eV. The maximum refractive indices of these structures then gradually decrease in the UV region, and the minimum value is 0.53 for all three structures, found at 28.5 eV. The non-zero and highest refractive index values of these compounds in the visible and near UV region, respectively suggest that these clinopyroxenes are not transparent to the incident photon energy in that region but can be transparent in the UV region at 28.5 eV where the refractive index is close to zero. The maximum extinction coefficients, $k(\omega)$, of these compounds, are very similar, around 1.1 at about 10 eV, meaning the highest ability to absorb photons in that region.

The dielectric function, often denoted by ε or $\varepsilon(\omega)$, is a fundamental concept in condensed matter physics and materials science. It describes how a material responds to an external electric field. The static peak of the dielectric function can give essential information

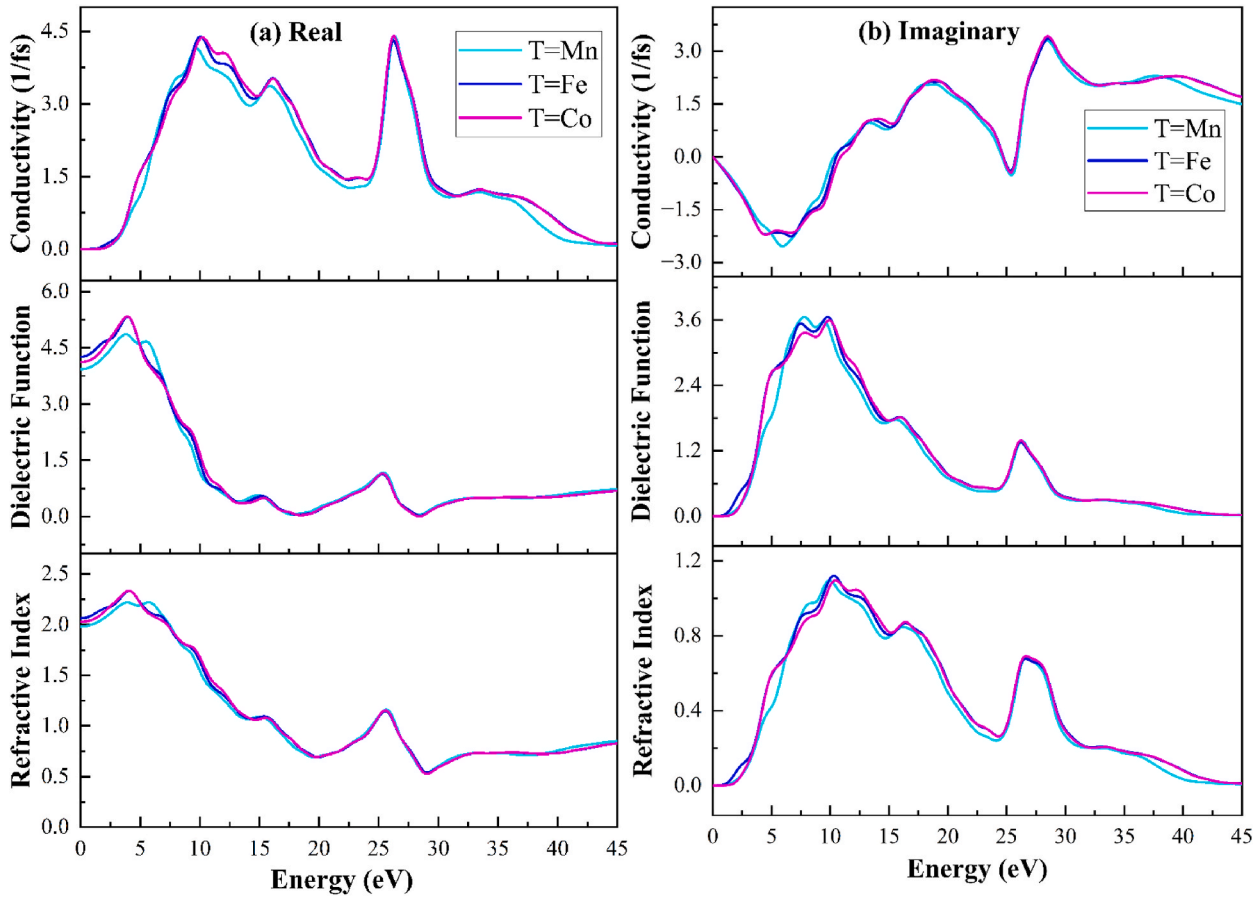

Fig. 6. (a) Real and (b) Imaginary portion of conductivity $\sigma(\omega)$, dielectric function $\varepsilon(\omega)$ and refractive index $n(\omega)$ of $CaTGe_2O_6$ (T = Mn, Fe, Co) as a function of photon energy from top to bottom respectively using GGA + U method.

about the efficiency of optoelectronic devices and the pace at which charge carriers recombine [59]. The dielectric function $\varepsilon(\omega)$ is thoroughly examined to comprehend $CaTGe_2O_6$ (T = Mn, Fe, Co) clinopyroxenes optical characteristics. Dielectric function $\varepsilon(\omega)$ has a real part $\varepsilon_1(\omega)$, which is directly connected to the real part of refractive indices and an imaginary part $\varepsilon_2(\omega)$ from where the absorption spectrum can be obtained. Also, the dielectric function refers to the representation of dielectric constants when expressed as a function of frequency. Dielectric constants determine a material's ability to store electric charges. The real and imaginary dielectric functions of the $CaTGe_2O_6$ (T = Mn, Fe, Co) clinopyroxenes are depicted in the middle layer of Figs. 6(a) and 5(b), respectively. The minimum value of the real dielectric functions of these compounds is zero at 17.5 eV and 28.3 eV. The refractive index's real part also has a minimum value near 28 eV. So, the dielectric functions and refractive indices ensure the transparency of $CaTGe_2O_6$ (T = Mn, Fe, Co) clinopyroxenes around 28 eV. $CaFeGe_2O_6$ and $CaCoGe_2O_6$ both possess the highest real dielectric function of 5.51 at 3.65 eV among the three structures, whereas the maximum value of the dielectric function (real) of $CaMnGe_2O_6$ is 5 at 3.57 eV. The peaks of the imaginary dielectric functions of $CaTGe_2O_6$ are around 3.71 at about 10 eV photon energy. In Fig. 6(a), the real part of the refractive indices (bottom layer) and the real part of the dielectric functions (middle layer) of the three compounds also show a similar pattern, as stated before.

Reflectivity is required for coating materials, indicating whether a material can be used as a coating substance. In Fig. 7, the middle layer reveals that reflectivity in the infrared region is around 0.12 and in the visible region is between 0.13 and 0.16. $CaFeGe_2O_6$ possesses the highest reflectivity of 0.20 at 10.25 eV among the three structures. However, at 28 eV, $CaCoGe_2O_6$ possesses the highest reflectivity of 0.18 among the three structures. These low reflectivity values suggest that these clinopyroxenes cannot be excellent reflecting coating material.

The top layer of Fig. 7 reveals the absorption spectra of these clinopyroxenes. The absorption coefficient of a material expresses the percentage attenuation of light strength per unit of passage through the medium [60]. These absorption spectra are negligible in the infrared and visible regions but significant in the ultraviolet region. $CaCoGe_2O_6$ and $CaMnGe_2O_6$ show a maximum absorption coefficient of 298×10^3 cm^{-1} at 26.5 eV. These results indicate that $CaMnGe_2O_6$ and $CaCoGe_2O_6$ clinopyroxenes can be sound absorbers in the UV region. The bottom layer of Fig. 7 depicts the frequency-dependent loss functions of these structures; at around 29 eV, these curves show peaks, where these materials sudden drop in absorption coefficient and reflectivity is also observed. This peak also goes by the name "plasmon peak" since it meets the requirements for plasma resonance at this photon energy [61].

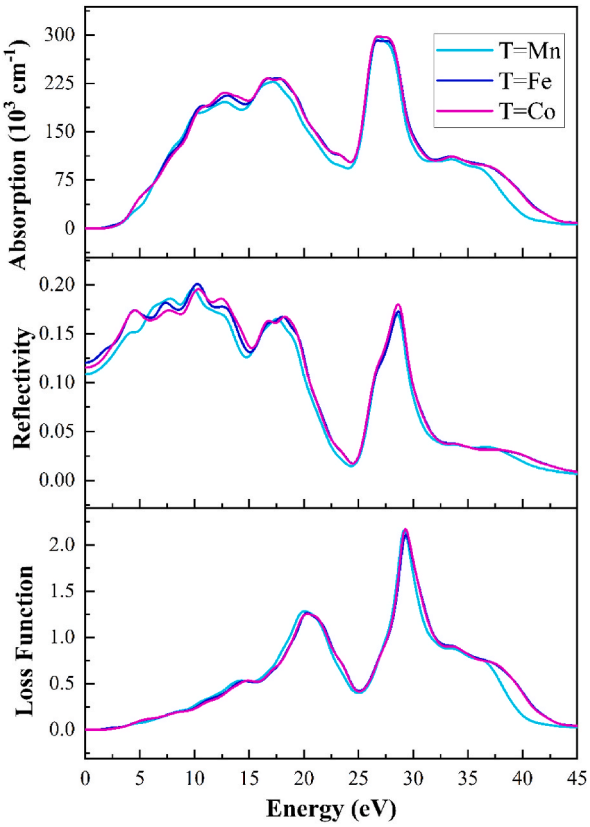

Fig. 7. Absorption coefficient α(ω), optical reflectivity R(ω), and loss function L(ω) of $CaTGe_2O_6$ (T = Mn, Fe, Co) from top to bottom, respectively using GGA + U method.

4. Conclusion

We have studied the first principle DFT analysis of the structural, mechanical, thermal, optical, and electronic characteristics of the monoclinic $CaTGe_2O_6$ (T = Mn, Fe, Co) clinopyroxenes using the CASTEP program. We have found that these clinopyroxenes have stable monoclinic structures, which can be confirmed by the evidence that the optimized lattice parameters of these structures are 1–6% greater than the experimental results. From the results of Pugh's ratio and Poisson's ratio of these structures, all three structures are found to be ductile in nature, and $CaCoGe_2O_6$ possesses the highest ductility. $CaMnGe_2O_6$ possesses the lowest volume stiffness according to VRH approximations. $CaCoGe_2O_6$ shows better lubricating properties, lower friction, and the highest plasticity among the three structures, as it has the most extensive machinability index. While considering the thermal properties (melting temperature, sound velocities, Debye temperature) of these structures, $CaFeGe_2O_6$ can be used in high-temperature applications and can be a good heat conductor. The half-metallic character of all three structures is confirmed by the spin-polarized PDOS and electronic band diagram. For $CaTGe_2O_6$ (T = Mn, Fe, Co), the half-metallic band gaps are 3.05, 1.69, 1.99 eV in GGA + U and 2.88, 1.52, 1.78 eV in LDA + U, respectively. $CaTGe_2O_6$ (T = Mn, Fe, Co) clinopyroxenes show high photoconductivity in the UV region. $CaMnGe_2O_6$ exhibits metallic behavior in the alpha spin channel, with the valence band crossing the Fermi level, and semiconducting behavior in the beta spin channel, where the valence and conduction bands do not touch the Fermi level. In contrast, $CaFeGe_2O_6$ and $CaCoGe_2O_6$ are metallic in the beta spin channel and semiconducting in the alpha spin channel. The non-zero and highest refractive indices of these structures are found in the visible and near UV region and then gradually decrease in the UV region, which suggests that these clinopyroxenes are not transparent to the incident photon energy in that region but can be transparent in the UV region at 28.5 eV. The dielectric functions of these structures also ensure the transparency of $CaTGe_2O_6$ (T = Mn, Fe, Co) clinopyroxenes around 28 eV. $CaFeGe_2O_6$ possesses the highest reflectivity, and the maximum absorption coefficient is found for $CaCoGe_2O_6$ and $CaMnGe_2O_6$ at 26.5 eV, which indicates that these two structures can be sound absorbers in the UV region. These structures' prominent characteristics imply that these clinopyroxene structures might prove useful in the future for the optoelectronics and spintronics sectors.

CRediT authorship contribution statement

Tasmi Akter: Writing – original draft, Visualization, Validation, Software, Methodology, Investigation, Formal analysis, Data curation, Conceptualization. **Jahirul Islam:** Writing – original draft, Validation, Supervision, Software, Methodology, Formal analysis,

Conceptualization. **Kamal Hossain:** Writing – review & editing, Validation, Supervision, Software, Methodology, Formal analysis, Conceptualization. **Rabeya Akter Rabu:** Writing – review & editing, Software, Formal analysis, Data curation.

Data availability

Data will be made available on request.

Declaration of competing interest

The authors declare that they have no known competing financial interests or personal relationships that could have appeared to influence the work reported in this paper.

Acknowledgments

The DFT simulations were performed in the Computational Materials Science Laboratory, Department of Materials Science and Engineering, Khulna University of Engineering & Technology, Khulna-9203, Bangladesh.

References

[1] J. Huidobro, et al., Geochemical characterization of the Martian analogues Enekuri and Fruiz, located in the Basque-Cantabrian Basin, by spectroscopic techniques, Sci. Total Environ. 905 (Dec. 2023) 167186, https://doi.org/10.1016/j.scitotenv.2023.167186.
[2] F.M. McCubbin, et al., Volatile abundances of coexisting merrillite and apatite in the martian meteorite Shergotty: implications for merrillite in hydrous magmas, Am. Mineral. 99 (7) (Jul. 2014) 1347–1354, https://doi.org/10.2138/am.2014.4782.
[3] C. Gong, E.M. Kim, Y. Wang, G. Lee, X. Zhang, Multiferroicity in atomic van der Waals heterostructures, Nat. Commun. 10 (1) (Jun. 2019) 2657, https://doi.org/10.1038/s41467-019-10693-0.
[4] I. Kim, B.-G. Jeon, D. Patil, S. Patil, G. Nénert, K.H. Kim, Observation of multiferroic properties in pyroxene NaFeGe2O6, J. Phys. Condens. Matter 24 (30) (Jul. 2012) 306001, https://doi.org/10.1088/0953-8984/24/30/306001.
[5] C.S. Lewis, et al., Synthesis, characterization, and growth mechanism of motifs of ultrathin cobalt-substituted $NaFeSi_2O_6$ nanowires, CrystEngComm 20 (2) (2018) 223–236, https://doi.org/10.1039/C7CE01885A.
[6] G.-K. Zhang, et al., Multiple magmatic processes revealed by distinct clinopyroxene populations in the magma plumbing system: a case study from a Miocene volcano in West Qinling, Central China, Am. Mineral. 109 (3) (Mar. 2023) 540–555, https://doi.org/10.2138/am-2022-8744.
[7] K. Hossain, R. Akter Rabu, Mst Shamima Khanom, M. Kamal Hossain, F. Ahmed, First-principles calculations to investigate effect of X+ cations variation on structural, mechanical, electronic and optical properties of the XCdCl3 chloroperovskites, Mater. Sci. Eng. B 289 (2023) 116228, https://doi.org/10.1016/j.mseb.2022.116228. Mar.
[8] Z. Yang, L.D. Spencer, H. Zhang, Z.L. Burmood, A. Putta, C. Jiang, Dynamic luminescence of lead-doped calcium zinc germanate clinopyroxene for multimode anticounterfeiting, ACS Appl. Mater. Interfaces 16 (13) (Apr. 2024) 16418–16426, https://doi.org/10.1021/acsami.3c16016.
[9] N.A. Shahed, S. Khanom, Md K. Hossain, F. Ahmed, Structural, mechanical, electronic and optical properties of half-metallic XFeSi2O6 (X = Li, Na, K) clinopyroxenes: a first-principles investigation, Mater. Sci. Eng. B 265 (Mar. 2021) 115026, https://doi.org/10.1016/j.mseb.2020.115026.
[10] G.J. Redhammer, et al., Nuclear and incommensurate magnetic structure of NaFeGe2O6 between 5 K and 298 K and new data on multiferroic NaFeSi2O6, Phys. Chem. Miner. 38 (2) (Feb. 2011) 139–157, https://doi.org/10.1007/s00269-010-0390-3.
[11] M. Isobe, E. Ninomiya, A.N. Vasil'ev, Y. Ueda, Novel phase transition in spin-1/2 linear chain systems: $NaTiSi_2O_6$ and $LiTiSi_2O_6$, J. Phys. Soc. Jpn. 71 (6) (Jun. 2002) 1423–1426, https://doi.org/10.1143/JPSJ.71.1423.
[12] G.J. Redhammer, H. Ohashi, G. Roth, Single-crystal structure refinement of NaTiSi2O6 clinopyroxene at low temperatures (298 < T < 100 K), Acta Crystallogr. B 59 (6) (Dec. 2003) 730–746, https://doi.org/10.1107/S0108768103022018.
[13] J.L. Gavilano, S. Mushkolaj, H.R. Ott, P. Millet, F. Mila, LiVGe 2 O 6 , an anomalous quasi-1D, S = 1 system, as revealed by NMR, Phys. Rev. Lett. 85 (2) (Jul. 2000) 409–412, https://doi.org/10.1103/PhysRevLett.85.409.
[14] Y. Sasago, M. Hase, K. Uchinokura, M. Tokunaga, N. Miura, Discovery of a spin-singlet ground state with an energy gap in CaCuGe 2 O 6, Phys. Rev. B 52 (5) (Aug. 1995) 3533–3539, https://doi.org/10.1103/PhysRevB.52.3533.
[15] S. Jodlauk, et al., Pyroxenes: a new class of multiferroics, J. Phys. Condens. Matter 19 (43) (Sep. 2007) 432201, https://doi.org/10.1088/0953-8984/19/43/432201.
[16] F. Fakhera, K. Hossain, Mst S. Khanom, M.K. Hossain, F. Ahmed, Understanding the impact of Y2+ (Y Mn, Fe, and Co) cations on physical properties of SrYGe2O6 clinopyroxene: a DFT insight, J. Phys. Chem. Solid. 173 (Feb. 2023) 111112, https://doi.org/10.1016/j.jpcs.2022.111112.
[17] F. Fakhera, N. Ahnaf Shahed, S. Khanom, M.K. Hossain, F. Ahmed, The first-principle study on structural, mechanical, electronic and optical properties of half-metallic CaMSi2O6 (M= Co, Fe, Mn) clinopyroxenes, Comput. Condens. Matter 33 (Dec. 2022) e00749, https://doi.org/10.1016/j.cocom.2022.e00749.
[18] B. Kerkeni, M.-C. Bacchus-Montabonel, X. Shan, S.T. Bromley, Understanding H2 formation on hydroxylated pyroxene nanoclusters: ab initio study of the reaction energetics and kinetics, J. Phys. Chem. A 123 (43) (Oct. 2019) 9282–9291, https://doi.org/10.1021/acs.jpca.9b06713.
[19] A. Torres, F.J. Luque, J. Tortajada, M.E. Arroyo-de Dompablo, Analysis of minerals as electrode materials for Ca-based rechargeable batteries, Sci. Rep. 9 (1) (Jul. 2019) 9644, https://doi.org/10.1038/s41598-019-46002-4.
[20] M. Legesse, H. Park, F. El Mellouhi, S.N. Rashkeev, S. Kais, F.H. Alharbi, Improved photoactivity of pyroxene silicates by cation substitutions, ChemPhysChem 19 (8) (Apr. 2018) 943–953, https://doi.org/10.1002/cphc.201701155.
[21] L. Ding, C.V. Colin, C. Darie, P. Bordet, SrMGe 2 O 6 (M = Mn, Co): a family of pyroxene compounds displaying multiferroicity, J. Mater. Chem. C 4 (19) (2016) 4236–4245, https://doi.org/10.1039/C6TC00149A.
[22] N.A. Shahed, S. Khanom, Md K. Hossain, F. Ahmed, Structural, mechanical, electronic and optical properties of half-metallic XFeSi2O6 (X = Li, Na, K) clinopyroxenes: a first-principles investigation, Mater. Sci. Eng. B 265 (Mar. 2021) 115026, https://doi.org/10.1016/j.mseb.2020.115026.
[23] G.J. Redhammer, et al., Magnetic ordering and spin structure in Ca-bearing clinopyroxenes CaM2+(Si, Ge)2O6, M=Fe, Ni, Co, Mn, J. Solid State Chem. 181 (11) (Nov. 2008) 3163–3176, https://doi.org/10.1016/j.jssc.2008.08.014.
[24] G.J. Redhammer, G. Roth, A. Senyshyn, G. Tippelt, C. Pietzonka, Crystal and magnetic spin structure of Germanium-Hedenbergite, CaFeGe2O6, and a comparison with other magnetic/magnetoelectric/multiferroic pyroxenes 228 (3) (Mar. 2013) 140–150, https://doi.org/10.1524/zkri.2013.1586.
[25] E. Lambruschi, et al., Raman spectroscopy of $CaM^{2+}Ge_2O_6$ (M^{2+} = Mg, Mn, Fe, Co, Ni, Zn) clinopyroxenes: Raman spectroscopy of $CaM^{2+}Ge_2O_6$, J. Raman Spectrosc. 46 (6) (Jun. 2015) 586–590, https://doi.org/10.1002/jrs.4681.
[26] M.D. Segall, et al., First-principles simulation: ideas, illustrations and the CASTEP code, J. Phys. Condens. Matter 14 (11) (Mar. 2002) 2717, https://doi.org/10.1088/0953-8984/14/11/301.
[27] J.D. Head, M.C. Zerner, A Broyden—Fletcher—Goldfarb—shanno optimization procedure for molecular geometries, Chem. Phys. Lett. 122 (3) (Dec. 1985) 264–270, https://doi.org/10.1016/0009-2614(85)80574-1.

[28] J.P. Perdew, K. Burke, M. Ernzerhof, Generalized gradient approximation made simple, Phys. Rev. Lett. 77 (18) (Oct. 1996) 3865–3868, https://doi.org/10.1103/PhysRevLett.77.3865.
[29] R.A. Evarestov, Modification of the Monkhorst-Pack special points meshes in the Brillouin zone for density functional theory and Hartree-Fock calculations, Phys. Rev. B 70 (23) (2004), https://doi.org/10.1103/PhysRevB.70.233101.
[30] J.P. Perdew, et al., Restoring the density-gradient expansion for exchange in solids and surfaces, Phys. Rev. Lett. 100 (13) (Apr. 2008) 136406, https://doi.org/10.1103/PhysRevLett.100.136406.
[31] D. Bhattarai, D.B. Shahi, M.P. Ghimire, Effect of hubbard potential (U) on Mn doped BiTeI, J. Nepal Phys. Soc. 9 (2) (Dec. 2023) 42–46, https://doi.org/10.3126/jnphyssoc.v9i2.62288.
[32] S. Sharma, S.K. Pandey, Effect of on-site Coulomb interaction (*U*) on the electronic and magnetic properties of Fe2MnSi, Fe2MnAl and Co2MnGe, J. Magn. Magn Mater. 403 (Apr. 2016) 1–7, https://doi.org/10.1016/j.jmmm.2015.11.069.
[33] J.J. Papike, C.T. Prewitt, S. Sueno, M. Cameron, Pyroxenes: comparisons of real and ideal structural topologies, Z. Für Krist. - Cryst. Mater. 138 (1–6) (Dec. 1973) 254–273, https://doi.org/10.1524/zkri.1973.138.jg.254.
[34] M. Segall, et al., First-principles simulation: ideas, illustrations and the CASTEP code, J. Phys. Condens. Matter 14 (Mar. 2002) 2717, https://doi.org/10.1088/0953-8984/14/11/301.
[35] J. Islam, K. Hossain, First-principles simulations to investigate effect of hydrostatic pressure on structural, mechanical, electronic, and optical properties of the AgCdCl3 perovskite, Emergent Mater 6 (6) (Dec. 2023) 1763–1777, https://doi.org/10.1007/s42247-023-00565-1.
[36] Md T. Hossain, J. Islam, M. Hasan, K. Hossain, First-principles calculation to investigate electronic, optical, and mechanical properties of halide perovskite LiABr3 (A = Ca, Sr, and Ba) for optoelectronic technologies, Phys. B Condens. Matter 691 (2024) 416355, https://doi.org/10.1016/j.physb.2024.416355. Oct.
[37] Y. Li, Y. Duan, M. Peng, S. Zheng, Structural, elastic, and thermal properties of TM5Si3C (TM = Ti, Cr, Y) carbides from first-principles calculations, Vacuum 218 (Dec. 2023) 112616, https://doi.org/10.1016/j.vacuum.2023.112616.
[38] M.A. Ali, A.A. Alothman, S. Mohammad, A. Khan, S.A. Khandy, M. Faizan, State of art in lead free double perovskite ceramics, X2MgTeO6 (X = Sr, Ba): structural stability and their potential energy harvesting applications, J. Inorg. Organomet. Polym. Mater. (May 2024), https://doi.org/10.1007/s10904-024-03115-2.
[39] M.D. Segall, R. Shah, C.J. Pickard, M.C. Payne, Population analysis of plane-wave electronic structure calculations of bulk materials, Phys. Rev. B 54 (23) (Dec. 1996) 16317–16320, https://doi.org/10.1103/PhysRevB.54.16317.
[40] M. Caid, Y. Rached, D. Rached, H. Rached, First principles study of the structural, elastic, magneto-electronic and thermoelectric properties of double perovskite Ba2ZrFeO6 in ferrimagnetic phase, Comput. Condens. Matter 37 (Dec. 2023) e00847, https://doi.org/10.1016/j.cocom.2023.e00847.
[41] A. Wederni, J. Daza, W. Ben Mbarek, J. Saurina, L. Escoda, J.-J. Suñol, Crystal structure and properties of heusler alloys: a comprehensive review, Metals 14 (6) (Jun. 2024), https://doi.org/10.3390/met14060688.
[42] J. Gao, Q.-J. Liu, B. Tang, Elastic stability criteria of seven crystal systems and their application under pressure: taking carbon as an example, J. Appl. Phys. 133 (13) (Apr. 2023) 135901, https://doi.org/10.1063/5.0139232.
[43] Md A. Rahman, R. Ferdous, D.C. Roy, R. Khatun, A. Irfan, Md F. Rahman, Pressure effect on the structural, electronic, mechanical, optical and thermal properties of Ga2TiX6 (X = Cl, Br): a DFT simulation, Mater. Sci. Eng. B 308 (2024) 117553, https://doi.org/10.1016/j.mseb.2024.117553. Oct.
[44] L. Zhang, H. Ahsbahs, S.S. Hafner, A. Kutoglu, Single-crystal compression and crystal structure of clinopyroxene up to 10 GPa, Am. Mineral. 82 (3–4) (Apr. 1997) 245–258, https://doi.org/10.2138/am-1997-3-402.
[45] Md H. Miah, et al., First-principles study of the structural, mechanical, electronic, optical, and elastic properties of non-toxic XGeBr3 (X=K, Rb, and Cs) perovskite for optoelectronic and radiation sensing applications, Mater. Chem. Phys. 319 (2024) 129377, https://doi.org/10.1016/j.matchemphys.2024.129377. Jun.
[46] L.-K. Gao, X.-S. Qi, Y.-L. Tang, First-principles study on the electronic structure, magnetic properties, elastic constants and sound velocity of the monoclinic crystal BiNiO3 under pressure, Results Phys. 58 (Mar. 2024) 107468, https://doi.org/10.1016/j.rinp.2024.107468.
[47] H. Mohapatra, C.J. Eckhardt, Elastic constants and related mechanical properties of the monoclinic polymorph of the carbamazepine molecular crystal, J. Phys. Chem. B 112 (8) (Feb. 2008) 2293–2298, https://doi.org/10.1021/jp077014c.
[48] S. Reza, M. Maaza, M.S. Islam, A computational study of the thortveitite structure of zinc pyrovanadate, $Zn_2\ V_2\ O_7$, under pressure, RSC Adv. 13 (25) (2023) 17212–17221, https://doi.org/10.1039/D3RA02426A.
[49] M.N. Mahamud Nobin, M. Khan, S. Saiful Islam, M. Lokman Ali, Pressure-induced physical properties in topological semi-metal TaM 2 (M = As, Sb), RSC Adv. 13 (32) (2023) 22088–22100, https://doi.org/10.1039/D3RA03085G.
[50] F. Fakhera, K. Hossain, S. Khanom, Md K. Hossain, F. Ahmed, Effect of pressure in tuning the physical properties of MAX phase Zr2AN (A = In, Ga): a DFT scheme, Results Phys. 53 (2023) 106912, https://doi.org/10.1016/j.rinp.2023.106912. Oct.
[51] E. Haque, M.A. Hossain, Elastic, magnetic, transport and electronic properties of noncentrosymmetric M2Mo3N (M = Fe, Co, Ni, Rh): a first-principles study, J. Alloys Compd. 748 (Jun. 2018) 117–126, https://doi.org/10.1016/j.jallcom.2018.03.151.
[52] M.L. Ali, M. Khan, M.A. Al Asad, M.Z. Rahaman, Highly efficient and stable lead-free cesium copper halide perovskites for optoelectronic applications: a DFT based study, Heliyon 9 (8) (Aug. 2023) e18816, https://doi.org/10.1016/j.heliyon.2023.e18816.
[53] M. Al-Fahdi, T. Ouyang, M. Hu, High-throughput computation of novel ternary B–C–N structures and carbon allotropes with electronic-level insights into superhard materials from machine learning, J. Mater. Chem. A 9 (48) (2021) 27596–27614, https://doi.org/10.1039/D1TA07553E.
[54] S.-B. Chen, S.-D. Guo, B. Lv, Y.S. Ang, Electronic, optical, elastic, and thermal properties of the half-Heusler-derived Ti2FeNiSb2: a DFT study, Phys. B Condens. Matter 689 (Sep. 2024) 416201, https://doi.org/10.1016/j.physb.2024.416201.
[55] O.L. Anderson, A simplified method for calculating the debye temperature from elastic constants, J. Phys. Chem. Solid. 24 (7) (Jul. 1963) 909–917, https://doi.org/10.1016/0022-3697(63)90067-2.
[56] M.I. Naher, S.H. Naqib, Structural, elastic, electronic, bonding, and optical properties of topological CaSn3 semimetal, J. Alloys Compd. 829 (Jul. 2020) 154509, https://doi.org/10.1016/j.jallcom.2020.154509.
[57] S. Skaftouros, Generalized Slater-Pauling rule for the inverse Heusler compounds, Phys. Rev. B 87 (2) (2013), https://doi.org/10.1103/PhysRevB.87.024420.
[58] M.K. Butt, M. Yaseen, A. Ghaffar, M. Zahid, First principle insight into the structural, optoelectronic, half metallic, and mechanical properties of cubic perovskite NdInO3, Arabian J. Sci. Eng. 45 (6) (Jun. 2020) 4967–4974, https://doi.org/10.1007/s13369-020-04576-6.
[59] X. Liu, et al., A high dielectric constant non-fullerene acceptor for efficient bulk-heterojunction organic solar cells, J. Mater. Chem. A 6 (2) (2018) 395–403, https://doi.org/10.1039/C7TA10136H.
[60] N.A. Shahed, M. Nishat, S. Khanom, M.K. Hossain, M.A. Hossain, F. Ahmed, Effect of oxygen deficiency on optical and magnetic properties of Ba2MMoO6 (M=Cr, Mn, Fe): a first-principles study, Comput. Condens. Matter 23 (Jun) (2020) e00464, https://doi.org/10.1016/j.cocom.2020.e00464.
[61] I. Zeba, et al., First-principles computation of magnesium doped CaZrO3 perovskite: a study of phase transformation, bandgap engineering and optical response for optoelectronic applications, Solid State Commun. 313 (Jun. 2020) 113907, https://doi.org/10.1016/j.ssc.2020.113907.